2009 American Control Conference
Hyatt Regency Riverfront, St. Louis, MO, USA
June 10-12, 2009

Modeling, Identification and Servo Control of Magnetic Medical Manipulator

İlker Tunay and Pablo Yoon

Abstract— **We describe modeling, system identification and control design for a magnet manipulator. Two of these manipulators, placed on either side of a patient, will articulate their large permanent magnets to generate a magnetic field in an anatomical region (e.g. the heart) as part of a medical navigation system under the remote control of a medical professional. We derive the equations of motion using the Lagrangian formulation; identify motor, amplifier and gear friction characteristics using data from a single manipulator prototype; design the servo control algorithm based on feedback linearization and decoupling followed by H_∞ control and test it on the prototype. Developing a mathematical model of the mechanism and using advanced controls algorithms initially take more time than tuning a PID controller. But the resulting design yields much smoother motor torques compared to high-gain controllers, does not excite high frequency dynamics and potentially improves reliability.**

I. Introduction

Our purpose is to design a model-based, multivariable servo control algorithm for the magnet manipulator shown in Fig. 1. Two of these manipulators, placed on either side of a patient, will articulate their large permanent magnets inside their pods to generate a magnetic field in an anatomical region (e.g. the heart) as part of a magnetic navigation system (MNS), intended to steer and navigate magnetic medical devices for diagnostic and therapeutic applications under the remote control of a medical professional, similar to a commercial system in current use [1].

The manipulator has three joints of articulation described with respect to an orthogonal frame attached to the magnet, with its z-axis perpendicular to the magnet front face and y-axis pointing up when the joints are at their reference (home) position, as shown in Fig. 1: A translation ζ positive in the z-axis direction, a rotation θ about the z-axis and a rotation ϕ about the y-axis. We will call these the "Navigation" joints to distinguish them from others (not shown) which are intended for repositioning the entire manipulator around the patient in an operating room, hence called "Support" joints. All Navigation joints are actuated by ac servo motors coupled to gear reducers. Motor angular positions are measured by absolute encoders. There are no specific velocity or acceleration sensors. Phi uses a drum and cable drive to rotate the magnet in its yoke; Theta has a slewing ring to rotate the yoke and the magnet; and Zeta uses a leadscrew to move the Theta carriage which contains all of the above. The case of the Phi reducer is attached to the Theta ring as shown in Fig. 2. This eliminates the need for an expensive and delicate slip ring to transmit Phi motor power and control signals, yet creates a mechanical coupling so that Theta rotation also results in Phi rotation in an amount divided by the Phi gear ratio, unless the Phi motor is rotated explicitly to compensate for it.

The controls designer faces several challenges in this mechanism: *i)* All joints are dynamically coupled in addition to the mechanical coupling mentioned above, hence a nonlinear multivariable system; *ii)* Gear reducers have significant friction with substantial stiction and Coulomb components; *iii)* Due to the weight (about 300 kg) of each magnet, there is considerable (nonlinear) gravitational loading; *iv)* a major part of the load is due to the magnetic interaction forces between the two manipulators, which are nonlinear and position dependent; and *v)* The cable drive, while lightweight, inexpensive and robust, introduces stretch into the system, hence reducing rigidity and limiting dynamic performance.

Our approach is similar to [2] and [3] in the way we combine feedback linearization with linear robust control. Alternatively, one may pursue adaptive control as in [4]. In what follows, we will derive the equations of motion in a Lagrangian framework; reduce the plant order via singular perturbation theory; describe the identification of cable, motor and gear friction characteristics from experimental data; design a servo control algorithm based on feedback linearization and decoupling followed by H_∞ control; and present experimental results on a prototype fixture (without a Zeta joint). We hope that our experience will be informative for the practicing controls engineer.

II. Magnet Manipulator Dynamics

We choose the degrees-of-freedom (DOF) as $q \stackrel{\text{def}}{=} [\zeta, \theta, \phi, \alpha]^T$, where α is the cable drum angular position. The potential energy is the sum of gravitational U_g and cable stretch U_s parts:

$$U_\text{g} = M_\text{M} g[(L_1 - \zeta + d_3 \cos\phi)\sin\gamma - d_3 \sin\phi \sin\theta \cos\gamma] + [M_\text{Q} g(L_1 - \zeta + d_1) + M_\text{OC} g(L_1 - \zeta + d_1 + d_2)]\sin\gamma\,, \tag{1}$$

where M_Q, M_M, M_OC are mass of yoke, magnet, and other components, γ is the pod tilt angle, and d_i, L_i are various distances. Since the cables between the Phi drum and magnet plate can only be stretched per the ratcheting preloading mechanism, their spring constants are combined into k, and

This work was entirely supported by Stereotaxis, Inc.

İ. Tunay is with Stereotaxis, Inc., 4320 Forest Park Ave, Suite 100 St. Louis, Missouri, 63108, USA, itunay@ieee.org

P. Yoon is with the Dept. of Electrical and Computer Engineering, University of Virginia, PO Box 400743, Charlottesville, VA 22904, USA

thus

$$U_{\mathrm{s}} = \frac{1}{2} k \left(\phi r_\phi - (\alpha - \theta) r_\alpha\right)^2 , \tag{2}$$

where r_α and r_θ are drum and magnet center plate radii.

The kinetic energy of the magnet, yoke and other drive components due to linear and angular motion is

$$\begin{aligned} T = \frac{1}{2}[&(M_{\mathrm{Q}} + M_{\mathrm{OC}})\dot{\zeta}^2 + \dot{\lambda}_1^2(I_{\mathrm{Z}} + I_{\mathrm{ZR}}) + \dot{\lambda}_2^2 I_{\mathrm{LS}} \\ &+ M_{\mathrm{M}}|\dot{\vec{R}}_{\mathrm{M}}|^2 + \dot{\beta}_1^2(I_{\mathrm{T}} + I_{\mathrm{TR1}}) + \dot{\beta}_2^2 I_{\mathrm{TR2}} + \dot{\theta}^2 I_{\mathrm{TS}} \\ &+ \dot{\alpha}_1^2(I_{\mathrm{P}} + I_{\mathrm{PR}}) + \dot{\alpha}^2 I_{\mathrm{PS}} + \vec{\omega}_{\mathrm{Q}}^T I^Q \vec{\omega}_{\mathrm{Q}} + \vec{\omega}_{\mathrm{M}}^T I^M \vec{\omega}_{\mathrm{M}} \end{aligned} \tag{3}$$

where I^M, I^Q are magnet and yoke inertias; N_{ZR}, P are ζ reducer ratio and leadscrew pitch; $I_{\mathrm{Z}}, I_{\mathrm{ZR}}, I_{\mathrm{LS}}$ are ζ motor, brake, reducer and leadscrew inertias; λ_1, λ_2 are ζ motor and reducer shaft positions; $N_{\mathrm{T1}}, N_{\mathrm{T2}}$ are θ first and second reducer ratios; $I_{\mathrm{T}}, I_{\mathrm{TR1}}, I_{\mathrm{TR2}}, I_{\mathrm{TS}}$ are θ motor, brake, reducer and shaft inertias; β_1, β_2 are θ motor and first reducer shaft positions; N_{P} is ϕ reducer ratio; $I_{\mathrm{P}}, I_{\mathrm{PR}}, I_{\mathrm{PS}}$ are ϕ motor, brake, reducer and shaft inertias; α_1, α are ϕ motor and reducer shaft positions; $\vec{R}_{\mathrm{M}}$ is the magnet position vector; $\vec{\omega}_{\mathrm{M}}, \vec{\omega}_{\mathrm{Q}}$ are magnet and yoke angular velocities, all of which can be expressed in terms of q_i and known constants. Using the mass matrix M the kinetic energy is rewritten as a quadratic function of the velocities $T = \frac{1}{2}\dot{q}^T M(q)\dot{q}$.

The motion of each DOF follows from $\frac{\mathrm{d}}{\mathrm{d}t}\left(\frac{\partial L}{\partial \dot{q}_i}\right) - \frac{\partial L}{\partial q_i} = f_i$ where the Lagrangian $L \stackrel{\mathrm{def}}{=} T - U$ and f_i is the external force acting on q_i. These forces consist of motor torques, magnetic interaction forces, gear friction and the kinematic coupling between the Phi reducer case and magnet yoke. Because of this coupling some of the Phi reducer input torque T_1 is transmitted to the Theta joint as $T_\theta = (N_{\mathrm{P}} - 1)T_1$. The Phi motor torque T_{P} is related to T_1 as $T_{\mathrm{P}} = T_1 + I_{\mathrm{P}}\ddot{\alpha}_1$, allowing us to substitute $T_\theta = (N_{\mathrm{P}} - 1)T_{\mathrm{P}} + (1 - N_{\mathrm{P}})I_{\mathrm{P}}\ddot{\alpha}_1$ and eliminate T_θ from equations of motion. The resulting dynamic equations are shown in Fig. 3.

In order to facilitate model reduction by the singular perturbation method [5], solve for the spring term $\phi r_\phi + r_\alpha(\theta - \alpha)$ in (7):

$$\begin{aligned} \phi r_\phi + r_\alpha(\theta - \alpha) = \frac{1}{k r_\alpha}\Big(&[N_{\mathrm{P}}^2(I_{\mathrm{P}} + I_{\mathrm{PR}}) + I_{\mathrm{PS}}]\ddot{\alpha} \\ &+ N_{\mathrm{P}}(I_{\mathrm{P}} + I_{\mathrm{PR}})(1 - N_{\mathrm{P}})\ddot{\theta} - N_{\mathrm{P}} T_{\mathrm{P}}\Big) . \end{aligned} \tag{8}$$

Then, substitute this term (8) into (5) and (6), eliminating k from those equations. Now, dividing (7) through by k and letting k$\rightarrow \infty$ eliminates the "fast dynamics" (7). The resulting quasi steady-state value of $\alpha = \theta + (r_\phi / r_\alpha)\phi$ is substituted into (5) and (6) to reveal the "slow dynamics," which is the rigid system without cable stretch. The exponential stability of the boundary layer is verified for the closed-loop system after the controller is inserted into the equations.

Although it is possible to work with the full model in Fig 3 for control design, the cable drum position α is not available for measurement, and there is a wide margin in the frequency domain between the slow and fast parts of the dynamics, as detailed in Sec. III. Therefore, we do not believe that the extra complexity of working with the full model is justifiable in view of the design requirements in Sec. IV.

Finally, we write the reduced dynamics in the compact form

$$M(q)\ddot{q} + C(q,\dot{q})\dot{q} + k(q) = Bu(t) + T_{\mathrm{m}}(q) - BT_f(\dot{q}) , \tag{9}$$

where the nonsingular matrix M contains mass and inertia terms, the C matrix represents Coriolis, Euler and centrifugal forces, k represents gravity and cable spring terms, u is motor torques, T_m is magnetic interaction torques at the magnet, T_f is friction referred to the motor shaft and the B matrix is torque conversion from motor to magnet, which is nonsingular because our system is fully actuated.

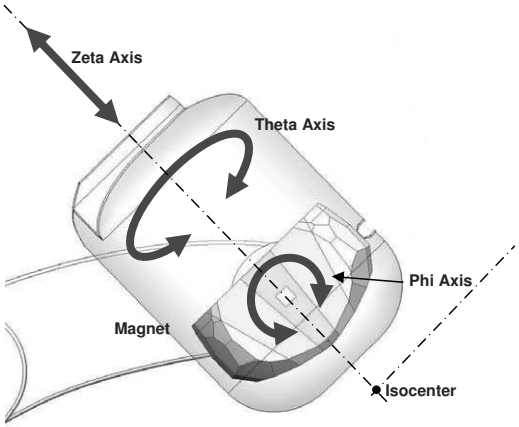

Fig. 1. The reference frame and magnet articulation joints.

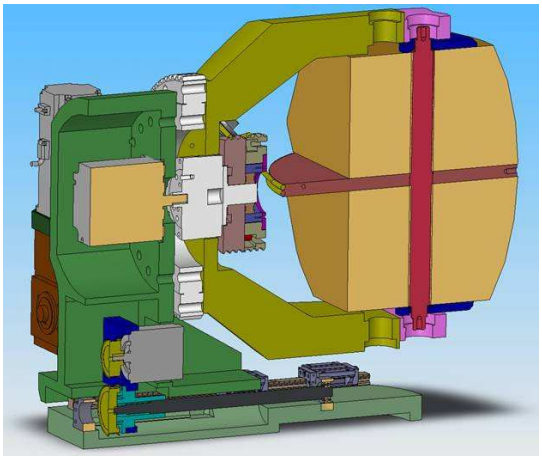

Fig. 2. Section view of Theta and Phi drive system.

$$\zeta \;:\; \left[M_{\mathrm{M}} + M_{\mathrm{Q}} + M_{\mathrm{OC}} + N_{\mathrm{Z}}^2 P^2 (I_{\mathrm{Z}} + I_{\mathrm{ZR}}) + P^2 I_{\mathrm{LS}}\right] \ddot{\zeta} + M_{\mathrm{M}} d_3 \sin(\phi)\, \ddot{\phi} + M_{\mathrm{M}} d_3 \cos(\phi)\, \dot{\phi}^2 - (M_{\mathrm{M}} + M_{\mathrm{Q}} + M_{\mathrm{OC}}) g \sin(\gamma) = N_{\mathrm{Z}} P T_{\mathrm{Z}} + F_{M\zeta} \tag{4}$$

$$\theta \;:\; [M_{\mathrm{M}} d_3^2 \sin^2(\phi) + N_{\mathrm{T1}}^2 N_{\mathrm{T2}}^2 (I_{\mathrm{T}} + I_{\mathrm{TR1}}) + N_{\mathrm{T2}}^2 (I_{\mathrm{TR2}}) + I_{\mathrm{TS}} + \sin^2(\phi) I_{\mathrm{x}}^{\mathrm{M}} + \cos^2(\phi) I_{\mathrm{z}}^{\mathrm{M}} + I_{\mathrm{z}}^{\mathrm{Q}} + (I_{\mathrm{P}} + I_{\mathrm{PR}})(N_{\mathrm{P}} - 1)^2]\ddot{\theta} + [N_{\mathrm{P}}(1 - N_{\mathrm{P}})(I_{\mathrm{P}} + I_{\mathrm{PR}})]\, \ddot{\alpha} + \left[2(M_{\mathrm{M}} d_3^2 + I_x^M - I_{\mathrm{z}}^{\mathrm{M}}) \sin(\phi) \cos(\phi)\right] \dot{\theta}\dot{\phi} + k r_\alpha \left(\phi r_\phi + r_\alpha(\theta - \alpha)\right) - M_{\mathrm{M}} g d_3 \sin(\phi) \cos(\gamma) \cos(\theta) = T_T + T_{M\theta} + (1 - N_{\mathrm{P}}) T_{\mathrm{P}} \tag{5}$$

$$\phi \;:\; \left[M_{\mathrm{M}} d_3 \sin(\phi)\right] \ddot{\zeta} + \left[M_{\mathrm{M}} d_3^2 + I_{\mathrm{y}}^{\mathrm{M}}\right] \ddot{\phi} - \cos(\phi) \sin(\phi)(M_{\mathrm{M}} d_3^2 + I_x^M - I_{\mathrm{z}}^{\mathrm{M}}) \dot{\theta}^2 + k r_\phi \left(\phi r_\phi + r_\alpha(\theta - \alpha)\right) - M_{\mathrm{M}} g d_3 (\sin(\phi) \sin(\gamma) + \sin(\theta) \cos(\phi) \cos(\gamma)) = T_{M\phi} \tag{6}$$

$$\alpha \;:\; \left[N_{\mathrm{P}}^2 (I_{\mathrm{P}} + I_{\mathrm{PR}}) + I_{\mathrm{PS}}\right] \ddot{\alpha} + N_{\mathrm{P}} (I_{\mathrm{P}} + I_{\mathrm{PR}})(1 - N_{\mathrm{P}}) \ddot{\theta} - k r_\alpha \left(\phi r_\phi + r_\alpha(\theta - \alpha)\right) = N_{\mathrm{P}} T_{\mathrm{P}} \tag{7}$$

Fig. 3. Equations of motion for the plant with cable stretch.

III. System Identification

Friction losses in gears, bearings and other sliding contacts in the mechanism must be estimated from experimental data since no theoretical procedure exists that can predict these reliably. Although gear manufacturers quote efficiency figures in their data sheets, these are often obtained from constant velocity operation with specific load conditions, hence have limited use in robotic applications. Also, stiction values are not quoted. Similarly, amplifier and motor gain characteristics are load dependent and manufacturer specifications must be cross checked with experiments. Finally, the cable stretch introduces an additional DOF into the system and the frequency of the associated mode in the model must be compared to the observations in order to guarantee control robustness.

We tested the motor and amplifier characteristics by attaching an inertia disk to the motor shaft with no other load and running profiles with constant desired acceleration under closed-loop servo control. The torque output of the motor was determined from the actual acceleration. The acceleration was computed from the measured position using the generalized derivative method which has much better noise immunity than centered finite differencing [6]. The computed acceleration was within 0.03% of the reference, indicating negligible following error. The current output of the amplifier was measured with a true-rms clamp meter and appeared 4% lower than the theoretical. The total gain from the DAC output to motor torque showed good linearity and was within 5% of the theoretical up to 5 Nm. For higher torques, the experimental gain was 9% less than the theoretical. These torque gain values show little variation with motor velocity up to 4000 rpm. In the model, we used the experimental amplifier-motor gain characteristics in a lookup table as a function of desired torque, instead of assuming a constant value.

Cable stretch is measured by a static loading test and by small-signal frequency response. For the former, we immobilized the magnet plate, increased the motor torque in small steps and measured the motor shaft position. Linear

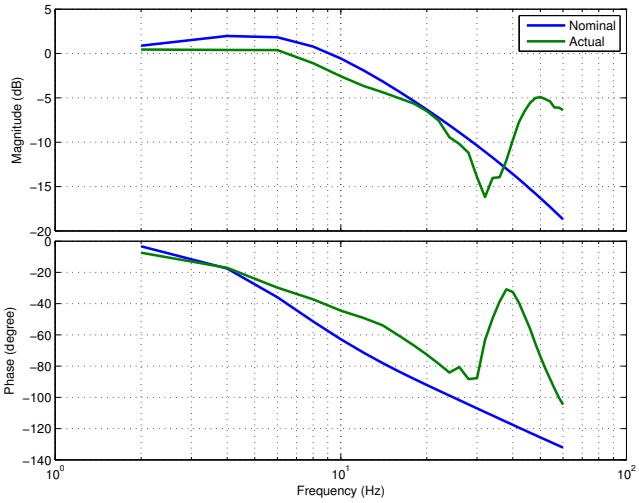

Fig. 4. Bode plot of nominal and actual systems from Phi reference to measured Phi position.

fitting of the data points show that the total compliance on Phi is 0.15 deg/Nm, which is in good agreement with the theoretical 0.14 deg/Nm derived from manufacturer's specifications. For the latter, we added a small amplitude constant frequency sinusoidal to a ramp reference going from -20 to 20 deg with constant velocity of 8 deg/sec and compared the magnitude and phase of the Fourier transforms at that frequency. In Fig. 4, the nominal is the closed-loop system with the springless plant without acceleration feedforward and the actual represents the measured data. The nominal and actual magnitude and phase plots match well until the effect of the pole-zero pair from cable flexibility becomes significant. The actual system has a bandwidth of about 10 Hz, and a magnitude peak at around 50 Hz due to the cable, which agrees with the theoretical resonant frequency of 54 Hz.

Stiction makes it difficult to position the load in small increments, and if integral control is used it can cause limit cycle oscillations around the set point. Stiction torque

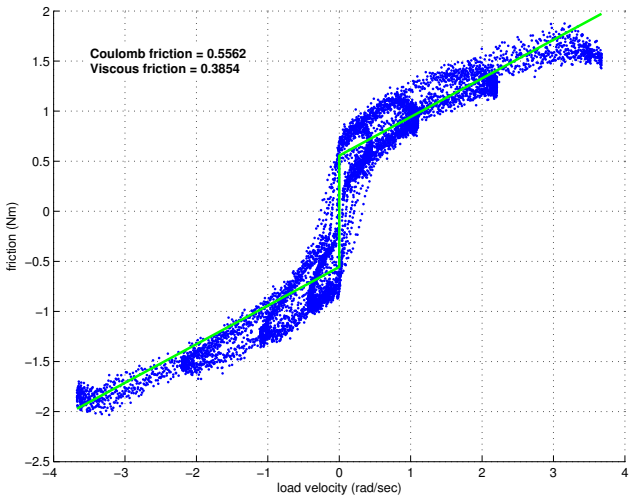

Fig. 5. Measured and fitted Phi friction vs. load velocity at 36 psi.

was determined by feeding a triangular reference signal of small amplitude and low frequency and by measuring the breakaway torque needed to start motion on both positive and negative directions. It was observed that stiction is position and direction dependent for both Theta and Phi joints and load dependent on Phi. The percentage motor torque needed to overcome stiction was less than 1.5% for Theta and less than 14% for Phi, which is quite significant.

Coulomb and viscous friction coefficients were estimated using a large sinusoidal reference signal with frequencies 0.05, 0.25 and 0.4 Hz. The load dependence was less significant in this case, but directonal dependence was significant. As observed in Fig. 5, this introduces hysteresis into the dynamics, similar to the Dahl friction model [7]. This is expected since gears with large ratios are difficult to backdrive and they may dissipate more heat when kinetic energy is being transferred from to load to the motor, i.e. during deceleration, compared to acceleration. Motor torque percentages used to overcome Coulomb friction was 11% for Phi and 4.4% for Theta. In all tests, stiction values were very close or less than Coulomb values. Motor torque needed for viscous friction depends on speed, and for rated load speed the percentages were 10% for Phi and 26% for Theta.

IV. Control Servo Algorithm Design

The proposed control servo algorithm (CSA) is based on the Computed Torque Control (CTC) scheme where the control law consists of two terms. The first is feedback linearization and decoupling [8] in which we precalculate the mass matrix, Coriolis matrix and the gravity vector to reduce the dynamics of each joint to a double integrator. Second, a linear controller is designed individually for each joint to satisfy tracking error, rise time, settling time, and disturbance rejection requirements while limiting controller bandwidth so as not to excite the cable dynamics. We formulate this as an H_∞ mixed sensitivity problem. All joint positions for linearization and feedback control are measured at the respective motor shaft. Magnet positions ζ, θ, ϕ are calculated from motor positions assuming that the plant is a stiff system. Instead of the actual load velocities, desired values are used.

The design requirements are *(i)* 10-90% rise time $t_\mathrm{r} \leq$ 100 ms; *(ii)* 1% settling time $t_\mathrm{s} \leq 300$ ms; *(iii)* steady-state error for ζ, θ and ϕ must be less than 0.375 mm, 0.375 deg and 0.75 deg respectively; *(iv)* tracking error for 0.5 Hz sinusoidal references of amplitudes 90^o for θ and 60^o for ϕ must be less or equal to the steady-state error; *(v)* absolute values of the joint velocities and accelerations are bounded; *(vi)* ζ is bounded above by a known smooth function of ϕ to keep the magnet in its cover.

These last two requirements are delegated to a separate path planning algorithm which operates at a much longer sampling period than the servo controller and uses cubic polynomials to interpolate at the servo rate using end point position, velocity and time values (PVT scheme). Because of the cubic representation, reference velocity and acceleration are available.

Consider the plant in (9) and assign the motor torques as

$$u = B^{-1}[C(q,\dot{q})\dot{q} + k(q) - \hat{T}_\mathrm{m}(q) + M(q)v(t) + M(q)\ddot{r}(t)] + \hat{T}_f(\dot{q}) \quad (10)$$

where r is reference position, $\hat{T}_\mathrm{m}$ is estimated magnetic torques, $\hat{T}_f$ is friction compensation, the error is $e(t) \stackrel{\mathrm{def}}{=} r(t) - q(t)$ and v is the output of the linear controller $v(t) = C(s)e(t)$ to be designed. Substituting (10) into (9) we get

$$\ddot{q} = \ddot{r} + v + d\,, \quad d \stackrel{\mathrm{def}}{=} M(q)^{-1}[\tilde{T}_\mathrm{m}(q) - B\tilde{T}_f(\dot{q})] \quad (11)$$

where d is disturbance, $\tilde{T}_\mathrm{m} \stackrel{\mathrm{def}}{=} T_\mathrm{m} - \hat{T}_\mathrm{m}$ and $\tilde{T}_f \stackrel{\mathrm{def}}{=} T_f - \hat{T}_f$. Figure 6 shows the resulting closed-loop system.

Let us ignore the coupling between the joints due to uncompensated magnetic interaction and friction forces in (11). Then $M = \mathrm{diag}[M_\zeta, M_\theta, M_\phi]$, $B = \mathrm{diag}[B_\zeta, B_\theta, B_\phi]$, and the linearized system for each joint becomes an independent single-input-single-output (SISO) double integrator $P(s) = 1/s^2$. Here we describe the process for designing the feedback controller for ϕ since the process for the others is identical. The output is $q = \phi$ and the error is $e = r - q$.

The sensitivity function is $S \stackrel{\mathrm{def}}{=} 1/(1+PC)$ and the complementary sensitivity is $T = 1 - S$. The closed-loop transfer functions from d to e is $-PS$, and from r to v is CS. Requirements *(iii)* and *(iv)* imply that $|P(j\omega)S(j\omega)||d| \leq 0.0087$ rad in the frequency range 0 to 0.5 Hz. Assuming a worst case $\tilde{T}_m$ of 20%, and assuming we compensate for 60% of total friction, we find that $|P(j\omega)S(j\omega)|$ must be bounded by -56 dB in that frequency range. We use the H_∞ scheme in [9] and [10] by selecting weights W_1 and W_2 as constants, W_3 as a first order low pass filter and W_4 as a first order high pass filter. The resulting closed-loop transfer function from input to output for the H_∞ synthesis becomes:

$$\begin{bmatrix} z_1 \\ z_2 \end{bmatrix} = \begin{bmatrix} W_3SW_1 & W_3PSW_2 \\ W_4CSW_1 & W_4TW_1 \end{bmatrix} \begin{bmatrix} \omega_1 \\ \omega_2 \end{bmatrix}, \quad (12)$$

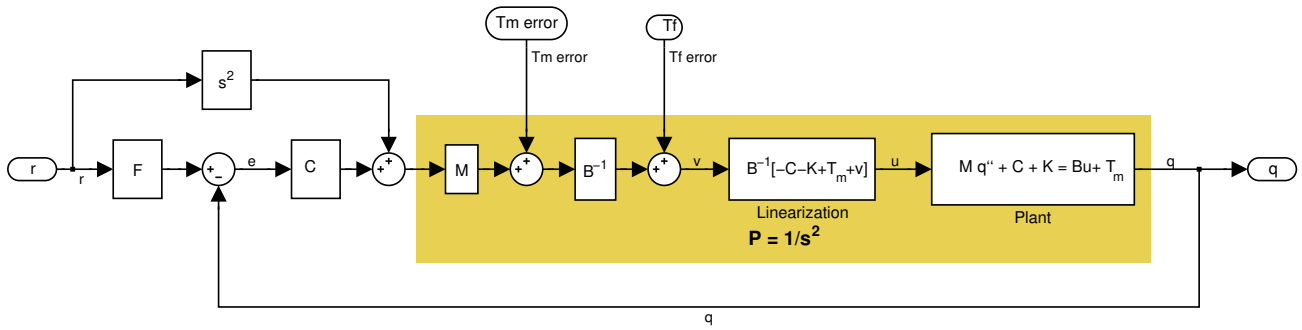

Fig. 6. Block diagram of the closed-loop system ($F(s) = 1$).

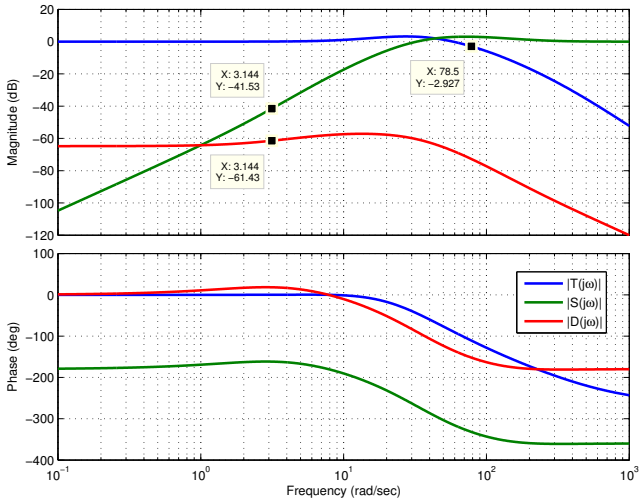

Fig. 7. Bode plot of the closed-loop system for the linearized double integrator plant P with the feedback filter C. T from reference to output (blue), $Sfrom$reference to error (green), and D from disturbance to error (red)

where $z_1 \stackrel{\text{def}}{=} W_3 e$ and $z_2 \stackrel{\text{def}}{=} W_4 v$.

After obtaining a satisfactory feedback filter from the H_∞ design to satisfy the requirements *(iii)* and *(iv)*, we analyze and modify the resulting controller using root-locus to satisfy time domain requirements *(i)* and *(ii)*. Figure 7 shows the Bode plots of the closed-loop transfer functions with the modified feedback filter, and we can see that it satisfies the disturbance rejection requirement on $PS(j\omega)$. The final linear feedback controller is

$$C(S) = \frac{2.6 \cdot 10^6 (s + 10.04)^2}{(s + 301)(s + 200.1)(s + 2.507)}. \qquad (13)$$

V. Experiment Results

Since the two manipulator system is not yet operational, the designed controller was tested on a test fixture with Theta and Phi joints only. The magnetic interaction was emulated by attaching a piston with compressed air to the magnet plate, which influences the Phi joint only. By adjusting the pressure and the lever arm geometry, the magnitude and position dependence of the air piston torque was made similar to the Phi magnetic torque. All collected data were obtained at 36 psi air pressure, which corresponds to maximum magnetic torque on Phi. The controller was discretized using pole-zero matching with a sampling period of 0.5 ms and implemented in C++ language, then converted to firmware and downloaded to Adept MotionBlox hardware which contains the motion control computer as well as amplifiers.

Figure 8 plots a 3 degree step response of Phi. The measured rise and settling times were 30 ms and 70 ms, respectively. There is a small amount of steady-state error due to stiction since we do not use integral control. But this error is within specifications.

Figure 9 shows Phi position error while tracking 60 deg, 0.5 Hz sinusoidal reference. Largest errors are observed when the sign of the Coulomb friction changes when motion changes direction, but they are within specifications. Figure 10 shows the corresponding motor torque, which is quite smooth.

We tried to tune a PID controller for this experimental system for comparison purposes, but were not able to get reasonable performance and maintain stability at the same time when the system had 36 psi air pressure. The previous generation system [1] uses PID control and it is instructive to see its Phi motor torque while tracking a smooth signal in Fig. 11. Note the large amount of chattering typical of high-gain control when measurement noise and drive train compliance are present.

VI. Conclusion

We have described model-based servo control design for a three DOF manipulator for a large magnet intended for medical navigation applications. The compliant cable drive, mechanical coupling beween two of the joints, substantial loading due to gravity and magnetic interaction forces, which necessitate high gear ratios, which in turn exhibit significant stiction and Coulomb friction, are some of the challenges that the controls designer faces. Developing a mathematical model of the mechanism and using advanced controls algorithms initially take more time than tuning a PID controller. But the resulting design yields much smoother motor torques compared to high-gain controllers, does not excite the cable dynamics, and potentially reduces component wear and improves reliability.

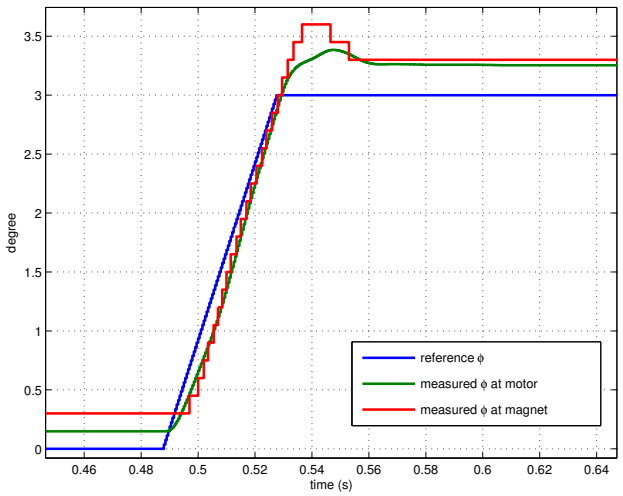

Fig. 8. Phi step response for test fixture. Blue is reference, green is ϕ measured at motor, and red is ϕ measured at load.

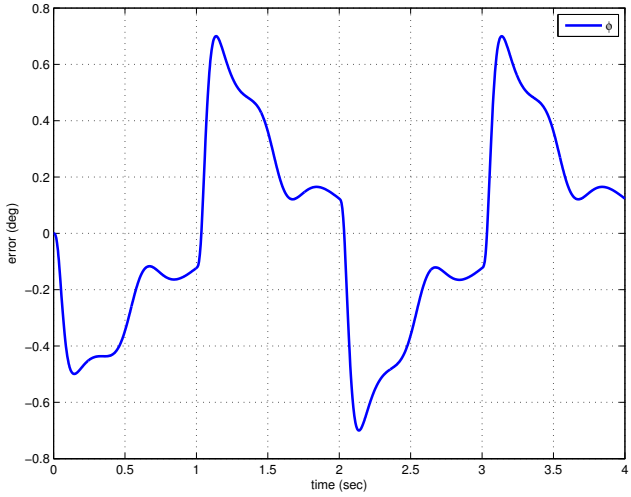

Fig. 9. Phi position error while tracking 60 deg, 0.5 Hz sinusoidal reference with the proposed method.

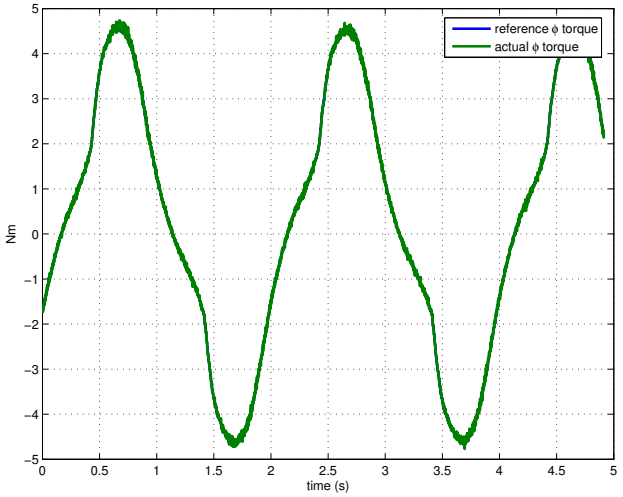

Fig. 10. Phi motor torque while tracking 60 deg, 0.5 Hz sinusoidal reference with the proposed method.

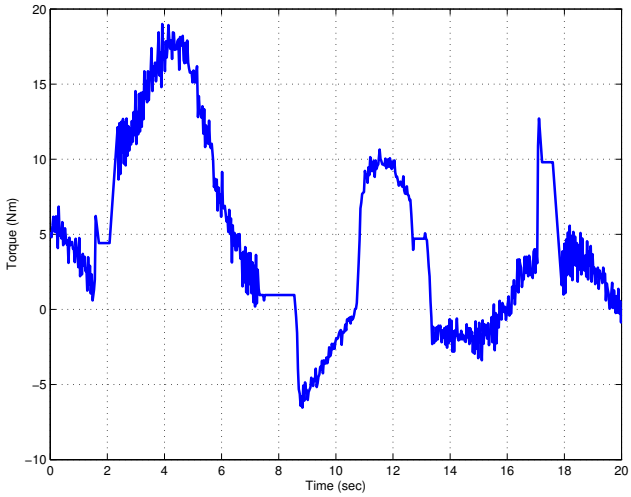

Fig. 11. Phi motor torque while tracking smooth reference with a PID controller for the previous generation system.

ACKNOWLEDGMENT

The authors would like to thank Stereotaxis for supporting this work entirely. From this company, Barbara Huen and Sandra Sowah helped with some of the earlier work on modeling and identification; Jim Morrow did C++ programming, firmware conversion, and testing on the hardware.

REFERENCES

[1] (2009, March) NIOBE Magnetic Navigation System. Stereotaxis, Inc. [Online]. Available: http://www.stereotaxis.com/Products-Technology/Magnetic-Navigation/

[2] İ. Tunay, E. Y. Rodin, and A. Beck, "Modeling and robust control design for aircraft brake hydraulics," *IEEE Trans. on Control Systems Technology*, vol. 9, no. 2, pp. 319–329, March 2001.

[3] A. Tchernychev, A. Sideris, and J. Yu, "Constrained H_∞ control of an experimental flexible link," *ASME Journal of Dynamic Systems, Measurement, and Control*, vol. 119, no. 2, pp. 206–211, June 1997.

[4] I. Kanellakopoulos, P. V. Kokotovic, and A. S. Morse, "Systematic design of adaptive controllers for feedback linearizable systems," *IEEE Trans. on Automatic Control*, vol. 36, no. 11, pp. 1241–1253, November 1991.

[5] H. K. Khalil, *Nonlinear Systems*, 2nd ed. New Jersey: Prentice-Hall, 1996.

[6] C. W. Groetsch, "Lanczos's generalized derivative," *American Mathematical Monthly*, vol. 105, no. 4, pp. 320–326, April 1998.

[7] G. Ferretti, G. Magnani, and P. Rocco, "Single and multistate integral friction models," *IEEE Trans. on Automatic Control*, vol. 49, no. 12, pp. 2292–2297, December 2004.

[8] A. Isidori, *Nonlinear Control Systems*, 3rd ed. London: Springer, 1995.

[9] L. Lublin, S. Grocott, and M. Athans, "h_2 and h_∞ control," in *The Control Handbook*. CRC Press, Inc., 1996.

[10] J. Doyle, K. Glover, P. P. Khargonekar, and B. A. Francis, "State space solutions to standard H_2 and H_∞ control problems," *IEEE Trans. on Automatic Control*, vol. 34, no. 8, pp. 831–847, August 1989.